Molecular Docking Interactions with Mycobacterial ATP and Polyketide-13 Synthase Enzymes of Phytoconstituents Isolated from *Entada abyssinica* Stem Bark

Samuel Baker Obakiro [1,2,3,*] ⓘ **, Isaac K'Owino** [3,4] **, Elizabeth Kigondu** [5] ⓘ **Moses Andima** [6] ⓘ **, Richard Oriko Owor** [6] ⓘ **, Ambrose Kiprop** [2,3] ⓘ

[1] Department of Pharmacology and Therapeutics, Faculty of Health Sciences, Busitema University P.O. Box 1460, Mbale, Uganda; sobakiro@gmail.com (S.B.O.);

[2] Department of Chemistry and Biochemistry, School of Sciences and Aerospace Studies, Moi University, P.O. Box 3900-30100, Eldoret, Kenya; ambkiprop@gmail.com (A.K.);

[3] Africa Centre of Excellence II in Phytochemicals, Textile and Renewable Energy (ACE II PTRE), Moi University, P.O. Box 3900-30100, Eldoret, Kenya; ambkiprop@gmail.com (A.K.);

[4] Department of Pure and Applied Chemistry, Faculty of Science, Masinde-Muliro University of Science and Technology, P.O. Box 190-50100, Kakamega, Kenya; ikowino@gmail.com (I.K.);

[5] Centre of Traditional Medicine and Drug Research, Kenya Medical Research Institute, P.O. Box 54840-00200, Nairobi, Kenya; ekigondu@kemri.org (E.K.);

[6] Department of Chemistry, Faculty of Science Education, Busitema University, P.O Box 236 Tororo Uganda; andima.moses@gmail.com (M.A.); richoriko@gmail.com (R.O.O).

* Correspondence: sobakiro@gmail.com (S.B.O.);

Abstract: The search for novel therapies for tuberculosis continues due to the emergence of resistant strains, adverse drug reactions, and potential drug-drug interactions of antitubercular drugs. This study was undertaken to identify compounds from *Entada abyssinica*, a plant used by herbalists in East Africa for the management of symptoms of tuberculosis. An extract of shade-dried *E. abyssinica* stem bark was prepared by maceration in a mixture of acetone and methanol in the ratio of 3:2. Column and thin layer chromatography were used to isolate pure compounds. The structures of the compounds were elucidated using nuclear magnetic resonance and infrared spectroscopy. The compounds were further studied using *in silico* tools to predict their binding affinities, descriptors of pharmacokinetics, and toxicity. Seven known compounds: 2,3-dihydroxypropyltriacontanoate (**1**), 1',26'-bis-(2,3-dihydroxypropyl) hexacosanedioate (**2**), stigmasterol 3-O-*β*-D-glucopyranoside (**3**), sitosterol 3-O-*β*-D-glucopyranoside (**4**), Spinasterol *3-O-β-D-*glucopyranoside (**5**), stigmasterol (**6**) and spinasterol (**7**) were isolated. Compounds **1** and **2** had better binding affinities (-27.7374 and -28.5726 Kcal/mol) than the bedaquiline (-22.9042 Kcal/mol) for ATP. All isolated compounds had better binding affinities (between -21.4357 and -18.7809 Kcal/mol) than isoniazid (-10.8307 Kcal/mol) for polyketide-13 synthase enzymes. The compounds showed variable but promising pharmacokinetic properties with minimum toxicity. *E. abyssinica* stem bark contains phytochemicals with promising antimycobacterial activity via inhibition of the ATP and polyketide-13 synthase enzymes. *In vitro* and *in vivo* studies are recommended to validate the predicted antimycobacterial activity as well as the pharmacokinetics and toxicity profiles.

Keywords: Fabaceae; tuberculosis; traditional medicine; drug discovery; pharmacokinetics; toxicity.

1. Introduction

Mycobacterium tuberculosis is a highly contagious and infectious pathogen that causes tuberculosis (TB), mainly affecting the pulmonary system and other extra-pulmonary organs [1]. Despite the enormous success registered in the "End TB strategy" globally, many countries in Africa, including Uganda, Kenya, and the United Republic of Tanzania, are ranked among the 30 countries with a high burden of TB in the world as of 2021 [2]. In 2020, a total of 1.5 million people died of TB worldwide compared to 1.4 million people in 2019. There is also an increasing emergence of resistant strains that have rendered the current therapies for TB less effective [3]. Additionally, the current therapies are associated with several toxicities and severe drug interactions with antiretroviral agents. Therefore, there is an urgent need to discover novel therapies against M. tuberculosis strains to effectively manage TB [4].

The discovery of novel molecules from medicinal plants continues to gain momentum due to their unlimited capacity to synthesize a variety of secondary metabolites with great pharmacological potential [5, 6]. In East Africa, *Entada abyssinica* A. Rich. (*E. abyssinica*) is among the plant species that have been documented to be widely used by traditional medicine practitioners to prepare herbal products for the management of symptoms of TB [7]. Additionally, the leaves, stem bark, and roots of this tree are harvested and used in the preparation of herbal remedies for the management of symptoms of other ailments such as ulcers, miscarriage, asthma, bacterial and fungal infections, malaria, snake bites, gastrointestinal discomfort and arthritis [8]. Several compounds isolated and characterized by this plant have been reported to exhibit good pharmacological activities [9-11]. For example, a new phenanthrene derivative (phenentada) isolated from this plant exhibited good antimicrobial activity with a minimum inhibitory concentration (MIC) of 3.12 µg/mL against both *Candida albicans* and *Salmonella enterica* [12]. The antimycobacterial activity of the crude leaf extracts of *E. abyssinica* has also been scientifically validated [13]. We also recently validated that the crude acetonic and methanolic stem bark extracts had antimycobacterial activity against *M. tuberculosis* with MIC of 937 ± 442 and 468 ± 22 µg/mL, respectively. However, crude extracts contain an array of phytochemicals with different functionalities that interact with each other pharmacologically with resultant synergistic and/or antagonistic effects [14]. Despite the promising antimycobacterial activities of crude extracts from *E. abyssinica*, few isolation and characterization studies have been undertaken to identify the active phytochemicals responsible for the antimycobacterial activity.

In silico or computational techniques are emerging tools used in the drug discovery process to fast-track the identification of potential leads [15]. These tools (software) provide a robust means of high throughput screening and assessment of the drug-like properties of compounds. These properties include absorption, distribution, metabolism, elimination, and toxicity. Other important properties, such as molecular weight, polar surface area (PSA), aqueous solubility, and molecular flexibility, can also be predicted [16]. Using these software (AutoDock, iGEMDOCK, OSIRIS property explorer, and admetSAR), bioactivity scores of potential leads against various molecular targets (enzymes and receptors) can also be predicted [17]. The tools can also be used to validate and optimize molecular targets to be used in docking studies. Therefore, this study was conducted to isolate and characterize phytochemicals from the stem bark of *E. abyssinica* and evaluate the drug-like properties and binding affinities against two selected molecular targets of *M. tuberculosis*. Herein, the isolation of monoglyceride fatty acids and phytosterols from the bark *E. abyssinica* and their molecular

docking interactions with mycobacterial ATP and Polyketide-13 synthase enzymes are reported.

2. Materials and Methods

2.1. Sample collection, authentication, and preparation.

The stem barks of *Entada abyssinica* were collected from Kisumu and Siaya counties, Western Kenya, with the help of a plant taxonomist. A voucher specimen (OSB/01/2020/001) was prepared and deposited at the University of Eldoret Herbarium, Botany Department, Eldoret (Kenya), for botanical authentication and reference purposes. The stem barks were collected in a clean sack and transported to the Moi Unversity Chemistry laboratory. They were cut into small pieces and dried at room temperature ($25.0 \pm 2.0°C$) to a constant mass in the laboratory for 28 days. They were then pulverized using an electric grinder (NutriBullet® 600 Series), packed, and stored in clean labeled paper envelopes at $25.0 \pm 2.0°C$.

2.2. Extraction and isolation of compounds.

The ground plant material (1 kg) was extracted with 4 L of a mixture of acetone and methanol (3:2) at room temperature for 24 hours. The extract was concentrated on a rotary evaporator at 40 °C under reduced pressure to obtain a brown crude extract (63 g). Thin layer chromatography analysis on crude extract was carried out in hexane/ethyl acetate/methanol at a ratio of 3:5:2. This revealed multiple spots when visualized under a UV lamp at 254 nm. The UV inactive phytochemicals were visualized by spraying with 5% sulphuric acid in methanol. The crude extract was adsorbed on 105 g of silica gel and loaded on a column (120 cm in length and 50 mm diameter) which was prepacked with a slurry of silica gel (500 g) in *n*-hexane. The column was then eluted with *n*-hexane/ethyl acetate, increasing amounts of ethyl acetate. Elution at 30% ethyl acetate yielded a white precipitate which was purified by vacuum filtration to yield a white solid SB-6B (6.8 mg), from which compounds **6** and **7** were identified. Elution with 50% ethyl acetate in *n*-hexane yielded a white precipitate which on drying gave a white amorphous solid of SB-10C (4.5 mg) from which compound **1** was identified. Elution at 100% ethyl acetate yielded a white precipitate washed with methanol to provide a white powder of SB-10F (5.2 mg), from which compounds **2, 3, 4,** and **5** were identified.

2.3. NMR analysis.

NMR spectra were recorded on a Bruker Advance III 600 MHz spectrometer equipped using standard pulse sequences and referenced with the TMS. The chemical shifts (δ) are expressed in parts per million (ppm) and coupling constants (*J*) in Hertz (Hz). COSY, NOESY, HSQC, and HMBC experiments were acquired using the standard Bruker programs. All the experiments were performed in deuterated solvents (CDCl$_3$ and DMSO), and chemical shifts were calibrated relative to the solvent peaks.

2.4. Fourier Transform Infrared (FTIR) Spectroscopy.

Infrared (IR) spectra were acquired using a JASCO FTIR - 6600 spectrometer (Japan) to determine the functional groups present in the samples by scanning them in the range between 4000 and 600 cm^{-1}.

2.5. Computational (in silico) studies.

In silico docking simulations were performed using the molecular operating environment (MOE) software version 2008.10 (Chemical Computing Group, Montreal, Canada). The London Gibbs free energy scoring function was used to predict the binding affinities in the MOE docking simulation with default settings. Proteins and ligands were prepared and checked before docking simulations were done, and the docking method was also validated for reproducibility and appropriateness.

2.5.1. Ligand preparation.

Seven compounds isolated from *E. abyssinica* were prepared for *in silico* studies. First, the 2D chemical structures of the isolated compounds (ligands) were drawn using Chembiodraw Ultra software, version 12.0 (Cambridge soft), and imported as SMILES string to generate 3D structures using the MOE structure builder tool. The Hamiltonian MMFF94X force field was applied to minimize the energy of the 3D molecules, and after, a local compound library was developed for docking simulations.

2.5.2. Protein preparation.

The crystal structures of ATPase (PDB ID: 3AR4) and polyketide synthase pks13 (PDB ID: 5V3Y) were downloaded from the protein data bank (PDB). These two proteins (enzymes) are critical in the pathogenesis of TB whereby ATPase is involved in energy release while pks 13 in mycolic acid biosynthesis. The molecular structures of the enzymes were prepared using the LigX tool in the MOE suite. After adding partial charges and protonating the amino acids, the crystal structures were sequentially minimized in three stages using the minimization protocol with default parameters. Finally, all water molecules and counter ions were deleted, and the binding sites were defined based on the co-crystallized ligands.

2.5.3. Docking method validation.

The docking method was validated by self-docking the co-crystallized ligands into the protein's binding site. During the docking, an induced-fit docking mode was adopted in which both the amino acid side chains in the binding site and ligand were left flexible to achieve an optimal fit. The root means square deviation (RMSD) upon superposition of the best-docked pose of the native ligand conformation was calculated and used to validate the appropriateness of the docking method. An RMSD value of less than 2Å was considered optimal. The binding affinities of the standard drugs measured in terms of S-score in Kcal/mol were used for comparison with the binding affinities of the test ligands (isolated compounds).

2.5.4. *In silico* docking of the compound library.

The compound library of the secondary metabolites was docked into the binding site of the target proteins. The S-score function was then used to rank the resultant docking poses of the ligands. If the S-score were more negative, it would imply that the binding affinity of the ligand to the target protein was strong. Isoniazid, rifampicin, and Bed aquiline (standard antitubercular drugs) were used as a positive control to compare the binding affinities of the isolated compounds.

2.5.5. Prediction of the drug-like properties of the isolated compounds.

The absorption, distribution, metabolism, elimination, and toxicity (ADMET) properties of the isolated compounds from *E. abyssinica* were computed using the open-source tools swissADME (http://www.swissadme.ch/) and ADMETLab 2.0 from computational Biology & Drug Design Group (https://admetmesh.scbdd.com/). This software is freely available online and robustly offers up-to-date and high-quality data [16]. ADMETLab 2.0 uses heterogeneous human epithelial colorectal adenocarcinoma cell lines (Caco2-cell) and Madin-Darby Canine Kidney (MDCK) cell models to calculate the oral drug absorption, human intestinal absorption, skin permeability, and transdermal drug absorption of the test compounds. Similarly, the program uses plasma protein binding and blood-brain barrier (BBB) penetration models to compute the distribution of the test compounds. The isolated compounds were input as SMILES, and the properties were calculated based on the algorithms [16].

3. Results

3.1. Isolation and identification of compounds.

Chromatographic separation of the crude acetone/methanol (3:2, v/v) extract of the stem bark of *E. abyssinica* led to the isolation and characterization of seven known compounds **1**-**7**. Compound **1** was isolated as a white powder, and its FTIR spectrum showed peaks for the hydroxy group (O-H) at 3262.46 cm^{-1} and carbonyl carbon (C=O) at 1636.07 cm^{-1} (Figure 1). NMR spectroscopic analysis revealed a monoacyl glycerol moiety [δ_H 4.08, dd, J = 11.7, 4.5 and 4.14, dd, J = 11.7, 6.1 (H-1); 3.86, m (H-2); 3.54, dd, J = 11.5, 5.8 and 3.63, dd, J = 11.5, 4.0 (H-3): δ_C 63.5 (C-1), 70.4 (C-2), 63.5 (C-3) and 174.5 (C-1')] (Table 1) [9]. Further, NMR spectra were dominated by a broad, intense peak at δ_H 1.20–1.54 and δ_C 25.1-29.9, indicating the presence of a long aliphatic methylene chain in the molecule. The presence of the methyl group was evident from NMR data that resonated at δ_H 0.81, t, J = 6.8, and δ_C 14.3. The methyl protons showed HMBC correlation with C-25' and a group of methylene carbons at C-5'-28'. The protons at δ_H 4.08 and 4.14 showed HMBC correlation with C-1', C-2, and C-3 confirming the presence of glycerol moiety. The HMBC of correlation of methylene protons at δ_H 2.28 with C-1' and C-4' provided a connection between the glycerol moiety and the long aliphatic methylene chain. Based on these spectral data, compound **1** was identified as 2,3-dihydroxypropyltriacontanoate (Figure 2). This compound was previously identified from the stem bark of this plant [18].

Table 1. ^{1}H (500 MHz), ^{13}C (125 MHz), and 2D-NMR data for compound **1** in CDCl$_3$

No.	δ_C	δ_H (mult., J in Hz)	HMBC
1	65.3 (CH$_2$)	4.08 (dd, *11.7, 4.5*) 4.14 (dd, *11.7, 6.1*)	C-2, C-3, C-1'
2	70.4 (CH)	3.86 (m)	1
3	63.5 (CH$_2$)	3.54 (dd, *11.5, 5.8*) 3.63 (dd, *11.5, 4.0*)	C-1, C-2
1'	174.5 (C=O)		
2'	34.3 (CH$_2$)	2.28 (t, *7.6*)	C-1', C-4'
3'	32.1 (CH$_2$)	1.20 (m)	C-2', C-5'-28'
4'	25.1 (CH$_2$)	1.54 (m)	C-2', C-5'-28'
5'-28'	29.3-29.9 (CH$_2$)$_{24}$	1.21 (m)	C-25', C-5'-28'
29'	22.8 (CH$_2$)	1.20 (m)	C-5'-28'
30'	14.3 (CH$_3$)	0.81 (t, *6.8*)	C-29', C-5'-28'
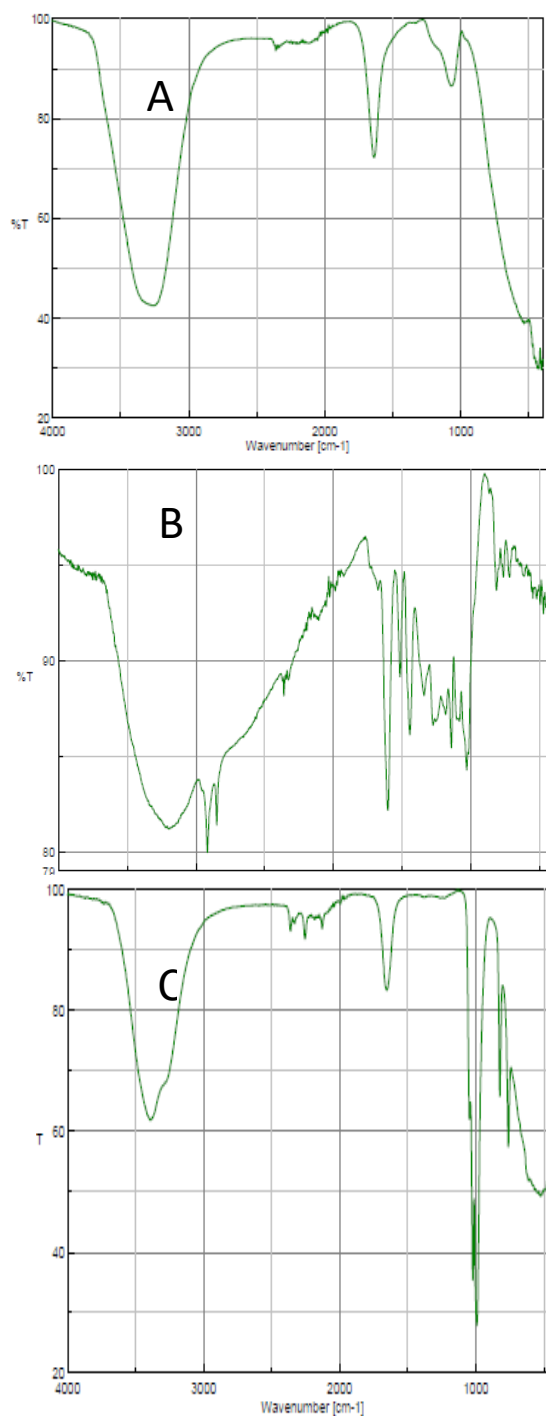
Figure 1. FTIR spectra of compounds identified in stem bark extract of *E. abyssinica*. (**A**) compound **1**; (**B**) Compounds **2**, **3**, **4,** and **5**, and (**C**) Compounds **6** and **7**.

Compound **2** was isolated as a mixture with compounds **3**, **4,** and **5**. The FTIR data showed peaks for the hydroxy group (O-H) at 3226.36 cm^{-1} and carbonyl carbon (C=O) at 1615.14 cm^{-1} (Figure 1). The NMR data [δ_H 4.03, dd, J = 11.1, 4.2 and 3.89, dd, J = 11.7, 6.5 (H-1/1"); 3.60, m (H-2/2") and 3.33, m (H-3/3"): δ_C 65.5 (C-1/1"), 69.3 (C-2/2"), 62.6 (C-3/3") and 172.3 (C-1'/26')] showed that compound **2** is a typical fatty acid glyceryl ester (Table 2)[9, 19]. Further, the NMR spectra were dominated by a broad, intense peak at δ_H 1.23 in ^{1}H NMR and δ_C 29.0 that supported the presence of a long aliphatic methylene chain [integrating to 20 (CH$_2$)] in this compound. As expected for a long chain monoacid derivative, the absence of methyl signals in 1H and 13C NMR spectra suggested that compound **2** is a symmetric dicarboxylic acid diester [9, 19]. The protons at δ_H 4.03 and 3.89 showed an HMBC correlation

with C-1'/26', C-2/2', and C-3/3', confirming the presence of glycerol moiety. Further, the proton at δ_H 1.51 also showed HMBC correlation with C-1'/26'. Based on these NMR data, compound **2** was identified as 1',26'-bis-(2,3-dihydroxypropyl) hexacosanedioate, also known as Tetracosanedioicacid-bis-(2,3-dihydoxypropyl)ester (Figure 1). This compound was previously identified in this plant [9, 11].
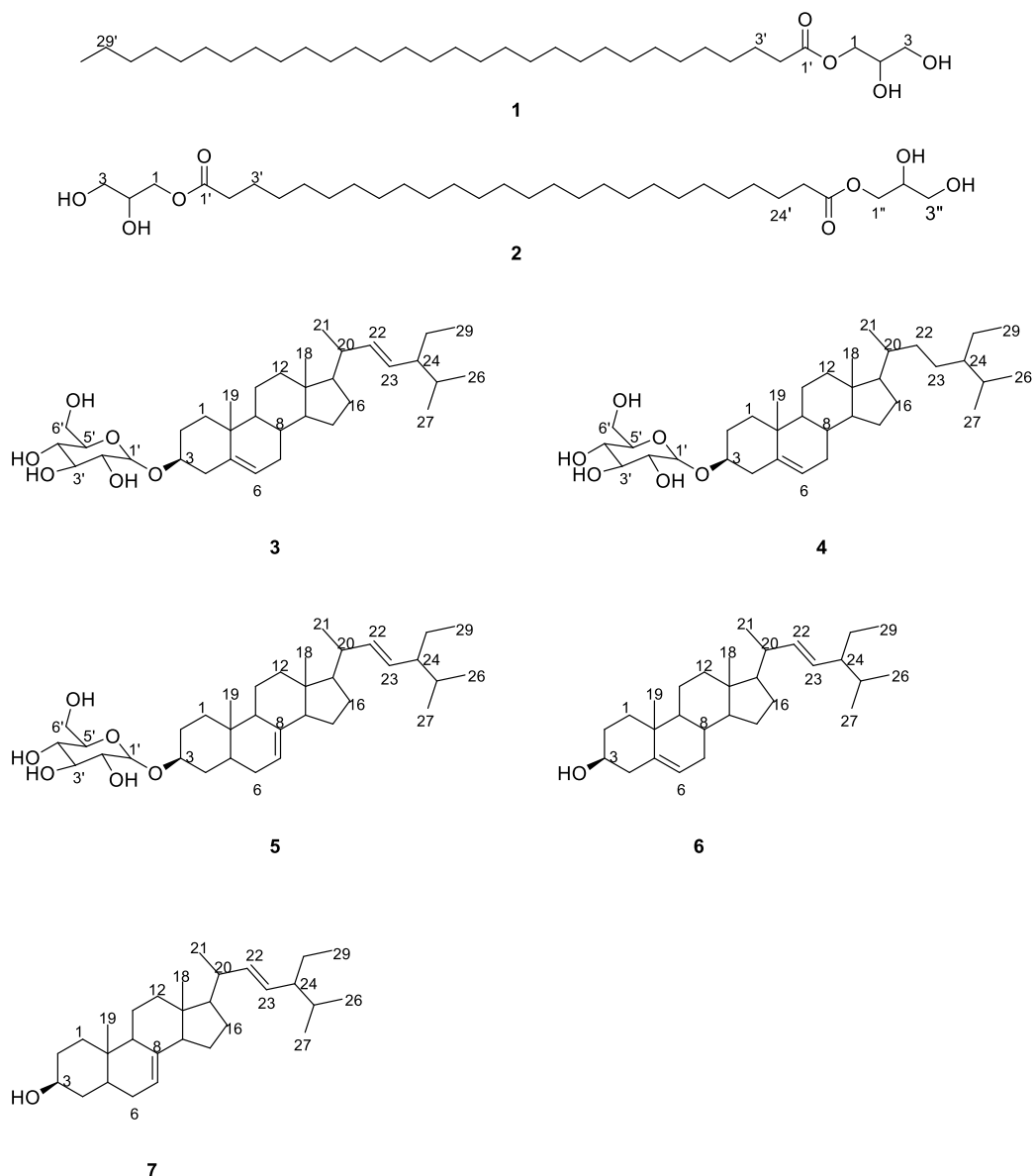

Figure 2. Structures of compounds isolated from acetone/methanol extract of *E. abyssinica* stem bark.

Table *2*. ^{1}H (500 MHz), ^{13}C (125 MHz), and 2D-NMR data for compound **2** in DMSO

No.	δ_C	δ_H (mult., *J* in Hz)	HMBC
1,1"	65.49 (CH$_2$)	4.03 (dd, *11.1, 4.2*) 3.89 (dd, *11.1, 6.5*)	C-2/2", C-3/3", C-1'/26'
2,2"	69.28 (CH)	3.60 (m)	C-1/1", C-3/3"
3,3"	62.63 (CH$_2$)	3.33, m	C-1/1", C-2/2"
1',26'	172.26 (C=O)		
2', 25'	33.48 (CH$_2$)	2.28 (t, *7.4*)	C-1'/26', C-3'/24', C-4'-23'
3',24'	24.45 (CH$_2$)	1.51 (m)	C-2'/25', C-1'/26'
4'-23'	29.02 (CH$_2$)$_{20}$	1.23 (broad-s)	C-4'-23', C-2'/25' C-3'/24'

Compound **3** was isolated as a mixture with compounds **2**, **4,** and **5**. The FTIR data showed peaks for the hydroxy group (O-H) at 3226.36 cm^{-1} and olefinic carbon (C=C) at 1485.17 cm^{-1} (Figure 1). The cholest-5-ene skeleton of compound 3 was evident from ^{13}CNMR

data (C$_5$: 140.5 and C$_6$: 121.2) (Table 3) [20-23]. Further, the NMR data revealed additional double [C-22 (δ_C 138.1) and C-23 (δ_C 129.0)] and glucoside moiety having anomeric carbon resonating at δ_C 100.7 (δ_H 4.22, dd, J = 7.8 Hz). The 1D- and 2D-NMR data of compound **3** are consistent with those reported in the literature, and therefore compound **3** was identified as stigmasterol *3-O-β-D*-glucopyranoside [20, 22]. This compound is widely distributed in several plant species and has been previously reported from *Acacia farnesiana* [24], *Prunella vulgaris* [20], [25], *Gomphrena globosa* [26], and *Nothopanax scutellarium* [27].

Compound **4** was isolated as a mixture with compounds **2**, **3,** and **5**. The FTIR data showed peaks for the hydroxy group (O-H) at 3226.36 cm^{-1} and olefinic carbon (C=C) at 1485.17 cm^{-1} (Figure 1). The cholest-5-ene skeleton of compound **4** was evident from ^{13}CNMR data (C$_5$: 140.5 and C$_6$: 121.2) (Table 3) [20-23]. Further, the NMR data of compound **4** were closely related to those of **3**. The only difference was the absence of an additional double bond [C-22 (δ_C 33.5) and C-23 (δ_C 25.4)]. The 1D- and 2D-NMR data of compound **4** are consistent with those reported in the literature. Thus, compound **4** was identified as *beta*-sitosterol *3-O-β-D*-glucopyranoside [28]. *Beta*-sitosterol *3-O-β-D*-glucopyranoside is widely distributed in plants, and it has been previously reported in plants such as *Alnus rugosa* [29] and *Verbena brasiliensis* [30].

Compound **5** was isolated as a mixture with compounds **2**, **3,** and **4**. The FTIR data showed peaks for hydroxyl group (O-H) at 3226.36 cm^{-1} and olefinic carbon (C=C) at 1485.17 cm^{-1} (Figure 1). The NMR data of compound **5** revealed cholest-7-ene skeleton [δ_C 117.2 for C-7 (δ_H 5.12, m, H-7) and 139.0 for C-8] (Table 3) [20]. The NMR data further revealed an additional double bond between C-22 (δ_C 137.9) and C-23 (δ_C 128.8). These 1D- and 2D-NMR data of compound **5** are consistent with those reported in the literature, and compound **5** was identified as spinasterol *3-O-β-D-* glucopyranoside [20, 31]. This compound is widely distributed in plants and has previously been reported in *Acacia concinna* [32] and *Prunella vulgaris* [20]. Compounds **3**, **4,** and **5** steryl monoglucosides (stigmasteryl, sitosteryl, and spinasteryl *β*-D-glucopyranoside) are also widely distributed in plants, and they have been previously isolated as mixtures [20, 25, 26, 33].

Table 3. ^{13}C NMR data (125 MHz) for compounds **3**–**7** in DMSO.

| No. | Compound | | | | |
| | 3 | 4 | 5 | 6 | 7 |
	δ_C	δ_C	δ_C	δ_C	δ_C
1	38.30	36.83	36.83	37.90	37.90
2	33.34	29.27	29.27	31.29	31.47
3	76.89	76.89	76.27	70.00	68.99
4	36.83	38.30	33.91	42.83	38.79
5	140.45	141.45	40.32	141.25	41.71
6	121.23	121.20	28.29	120.38	28.54
7	31.37	31.34	117.22	31.42	117.24
8	31.37	31.34	139.02	31.42	139.03
9	49.60	49.60	48.65	50.60	49.61
10	36.23	36.23	33.48	36.69	33.81
11	22.60	20.95	22.62	21.03	22.09
12	38.76	38.76	38.86	38.79	38.79
13	41.86	41.75	41.75	42.22	42.83
14	56.26	56.17	55.18	56.28	54.49
15	24.89	23.88	23.88	24.36	23.89
16	29.27	27.80	28.47	28.99	28.50
17	55.42	55.34	56.17	55.33	55.33
18	11.80	11.69	12.14	12.14	11.88
19	18.94	19.11	12.81	19.73	13.96
20	35.49	35.49	41.20	40.49	42.22
21	18.62	18.62	19.11	21.25	21.03

No.	Compound				
	3	4	5	6	7
	δ_C	δ_C	δ_C	δ_C	δ_C
22	138.06	33.48	137.94	137.94	138.06
23	128.97	25.42	128.82	128.96	128.86
24	31.42	45.13	50.59	50.60	50.60
25	31.42	28.47	31.37	31.90	31.34
26	19.11	18.94	21.25	19.11	21.25
27	18.85	22.06	21.11	19.03	18.93
28	23.88	22.06	25.42	25.41	25.41
29	11.69	11.79	11.80	12.88	12.14
1'	100.77	100.77	100.84		
2'	73.47	73.47	73.47		
3'	76.77	76.77	76.77		
4'	70.10	70.10	70.10		
5'	76.74	76.74	76.74		
6'	61.10	61.10	61.10		

Compound **6** was isolated as a mixture with compound **7**. The FTIR data showed peaks for the hydroxy group (O-H) at 3310.73 cm^{-1} and olefinic carbon (C=C) at 1634.09 cm^{-1} (Figure 1). The cholest-5-ene skeleton of compound 3 was evident from ^{13}C NMR data (C$_5$: 141.3 and C$_6$: 120.4) (Table 3) [20-23]. The NMR data of compound 6 is closely related to compound 3. The only difference was the absence of glucoside moiety. The 1D- and 2D-NMR data of compound 6 are consistent with those reported in the literature, and compound **6** was identified as stigmasterol [20, 22]. This compound is widely distributed in many plants, and it was previously reported in *Acacia farnesiana* [24], *Prunella vulgaris* [20, 25], *Gomphrena globosa* [26], and *Nothopanax scutellarium* [27].

Compound **7** was isolated as a mixture with compound **6**. The FTIR data showed peaks for the hydroxy group (O-H) at 3310.73 cm^{-1} and olefinic carbon (C=C) at 1634.09 cm^{-1} (Figure 1). The NMR data of compound **7** revealed cholest-7-ene skeleton [δ_C 117.2 for C-7 (δ_H 5.11, m, H-7) and 139.0 for C-8] (Table 3) [20]. The NMR data of compound **7** is closely related to compound 5. The only difference was the absence of glucoside moiety. The 1D- and 2D-NMR data of compound 7 are consistent with those reported in the literature, and it was identified as a spinasterol [34]. This compound is widely distributed in many plants, and it was previously reported in *Stegnosperma halimifolium* [34], *Citrullus Colocynthis* [35], *Amaranthus spinosus* [36], and *Phytolacca americana* [37].

3.2. In silico screening results.

Self-docking of the co-crystalized ligand into the binding sites of the molecular targets resulted in root mean square deviation values of less than 2 Å (Table 4). This implied that the docking method was appropriate and reproducible (Figures 3 and 4).

Table 4. The root means square deviation (RSMD) and binding affinities of the re-docked co-crystalized ligands.

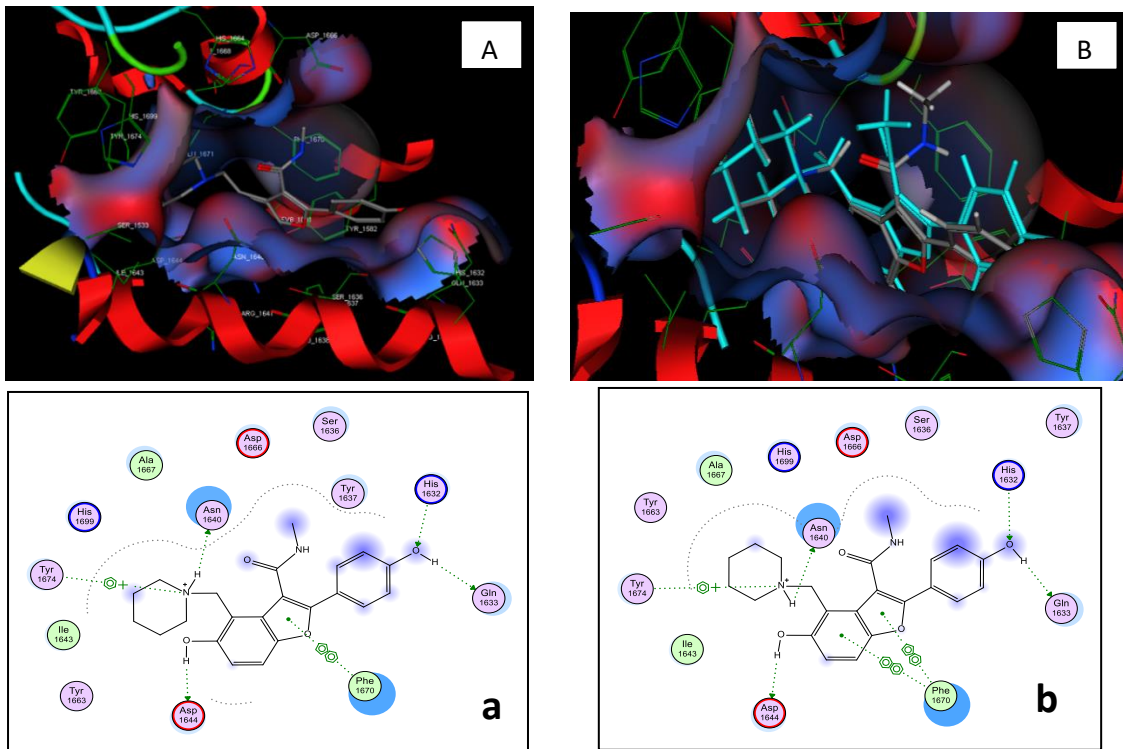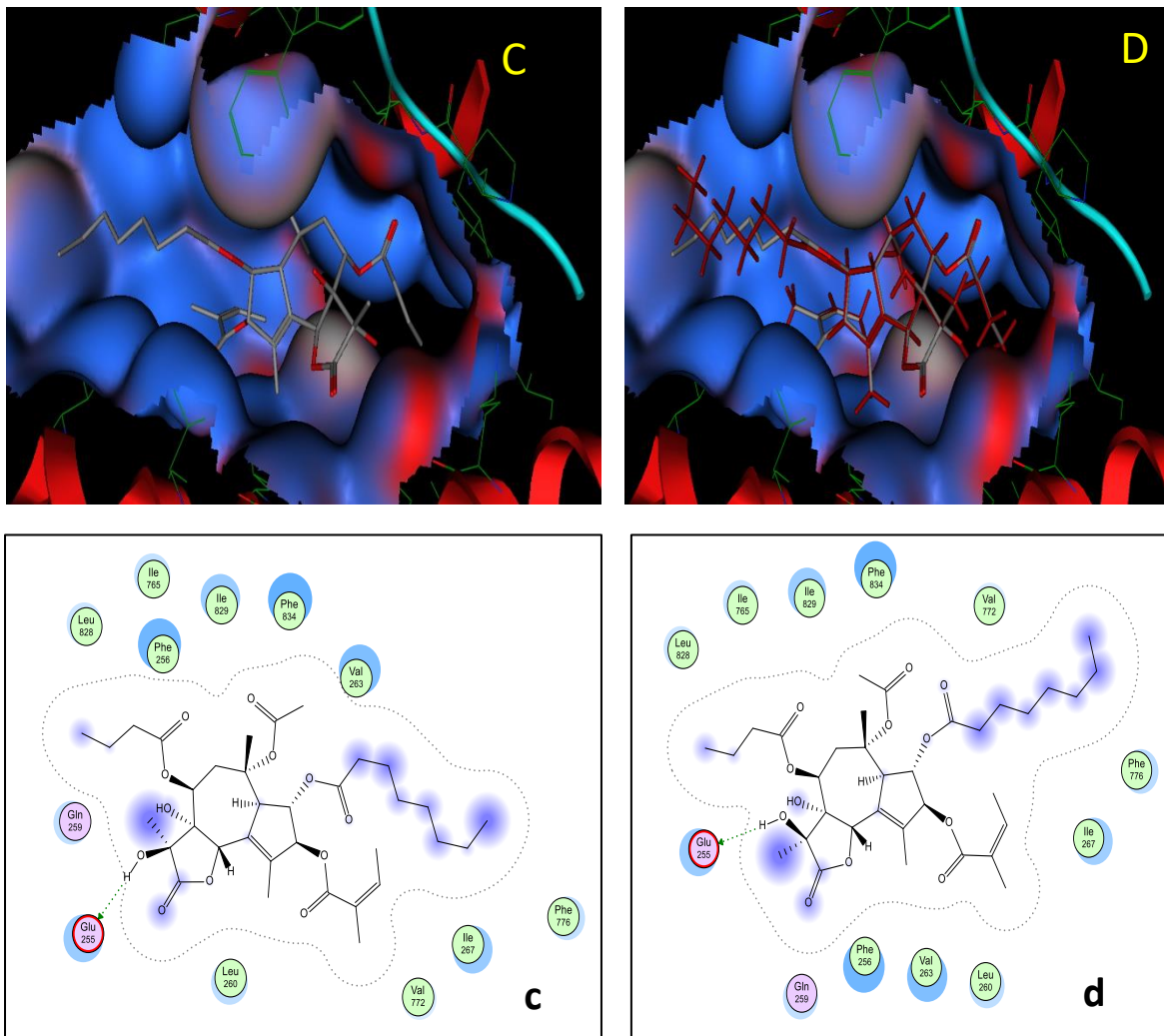| Target (PDB ID)	RMSD	Binding energy (Kcal/mol)
Polyketide synthase 13 (5V3Y)	0.8288	-28.2653
ATP synthase (3A4R)	0.7076	-37.9922

Figure 3. Maps of the pose for (**A**) co-crystallized ligand in the binding site of polyketide synthase -13 and (**B**) re-docked pose of co-crystalized ligand superposed on the native ligand. (**a**) Interactions of co-crystalized ligand in the binding site of polyketide synthase -13;(**b**) Interactions of co-crystalized ligand superposed on the native ligand re-docked pose.
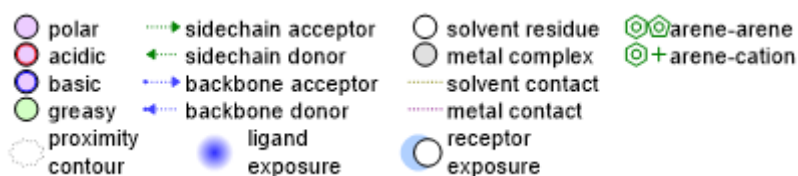
polar — ▸ sidechain acceptor ○ solvent residue ⊙⊙ arene-arene
acidic ◂— sidechain donor ○ metal complex ⊙+ arene-cation
basic ⋯▸ backbone acceptor solvent contact
greasy ◂⋯ backbone donor metal contact
proximity ligand receptor
contour exposure exposure

Figure 4. Maps of the pose of (**C**) co-crystalized ligand in the binding of ATP synthase and (**D**) re-docked pose of co-crystalized ligand superposed on the native ligand. (**c**) Interactions of co-crystalized ligand in the binding of ATP synthase; (**d**) Interactions of co-crystalized ligand superposed on the native ligand re-docked pose.

3.3. Binding affinities of the isolated compounds from E. abyssinica for polyketide synthase and ATP synthase enzymes.

The isolated compounds exhibited sufficient binding affinities for the two targets that were better than those of the standard drugs (Isoniazid and rifampicin) that form the backbone of the first-line TB regimen (Table 5).

Table 5. Binding affinities for the isolated compounds from *E. abyssinica* stem bark against selected *M. tuberculosis* targets.

Isolated compound	Binding energy (Kcal/mol)	
	ATP synthase	Polyketide synthase - 13
2,3-dihydroxypropyltriacontanoate (**1**)	-27.7374	-21.4357
1',26'-bis-(2,3-dihydroxypropyl)hexacosanedioate (**2**)	-28.5726	-18.4978
Stigmasterol *3-O-β-D*-glucopyranoside (**3**)	-21.2349	-17.6151
Sitosterol *3-O-β-D*-glucopyranoside (**4**)	-23.7580	-18. 8397
Spinasterol *3-O-β-D*- glucopyranoside (**5**)	-22.5131	-18.7809
Stigmasterol (**6**)	-12.9573	-7.9024
Spinasterol (**7**)	-15.1663	-12.8924
Bedaquiline	-22.9042	-24.0017
Isoniazid	-11.6257	-10.8307
Rifampicin	-18.5886	-17.5541

3.4. Pharmacokinetic and toxicity evaluation (ADMET descriptors).

Descriptor parameters of pharmacokinetics and toxicity for the isolated compounds were computed to give an insight into the drug-like properties of the compounds. If the compounds possess optimal ADMET properties, then the compounds are suitable candidates for developing potential leads. However, compounds with sub-optimal ADMET properties might require optimization to enhance their drugability. Among the ADME descriptors that were calculated included water-solubility, human intestinal absorption, plasma protein binding (PPB), blood-brain barrier (BBB) penetration, CYPP450 inhibition, Volume of distribution (VD), Clearance, half-life, and skin permeation. The different toxicity parameters were also calculated to predict the likelihood of toxicity, including AMES toxicity, hERG blockers, hepatotoxicity, and skin sensitization. The results are presented in Table 6.

4. Discussion

4.1. Antibacterial activity of the isolated compounds.

An extensive literature search was conducted in various online databases (Scopus, Google Scholar, Science Direct, Springer Link, PubChem, PubMed & the Google Search Engine) to identify if there are reported antibacterial activity of the isolated compounds using their IUPAC and other names from NIST webbook and PubChem. The study indeed found out

that only compound 2 (1',26'-bis-(2,3-dihydroxypropyl) hexacosanedioate) does not have reported antibacterial activity.

Sitosterol 3-O-β-D-glucopyranoside (4) was reported to have shown antimycobacterial activity with MIC of 62.5 μg/mL against Isoniazid-resistant strain of *M. tuberculosis* (AC45). Further, it exhibited antimycobacterial activity against clinical isolates of M. tuberculosis with MIC of 62.5 μg/mL and MBC of 125 μg/mL [38]. A beta version of this compound (β-sitosterol 3-O-β-D-glucopyranoside) showed antibacterial activity against *Staphylococcus aureus, Bacillus cereus, Pseudomonas aeruginosa*, and *Salmonella typhi* with zone inhibition diameter (ZOI) of 8.0, 10.5, 10.5 and 10.0 mm at 2 mg/mL, respectively [39]. It was also reported that 3-O-β-D-sitosterol glucopyranoside exhibited antibacterial activity against *Staphylococcus aureus, Streptococcus faecalis, Pseudomonas aeruginosa*, and *Shigella flexneri* with MIC of 12.5, 6.3, 3.2 and 12.5 μg/mL, respectively [40]. The same compound was reported to show antibacterial activity against *Bacillus subtilis, S. aureus*, and *Micrococcus luteus* with MIC values of 50, 200, and 400 μg/mL, respectively [41]. Stigmasterol (6)showed antimycobacterial activity against *M. tuberculosis* (H37Rv) with MIC ranging between 100 and 128 μg/mL [42, 43]. It was also active against *M. smegmatis* with MIC of 500 μg/mL [44, 45]. Compound 6 inhibited the growth of several bacteria such as *Methicillin-resistant S. aureus* (ZOI = 30 mm), *S. aureus* (ZOI = 29 mm), *Streptococcus faecalis* (ZOI = 27 mm), *E. coli* (ZOI = 24 mm) and *Pseudomonas fluorescens* (ZOI = 23 mm) [46]. This compound was also demonstrated to inhibit the growth of *S. aureus, E. coli, P. aeruginosa,* and *Salmonella typhimurium* with ZOI of 12, 18, 11, and 13 mm, respectively [47].

Table 6. Predicted parameters for the ADMET properties of the isolated compounds.

ADMET Property	Isolated compound							
	1	2	3	4	5	6	7	Acceptable values
Absorption								
Water solubility (Log S)	-9.76	-6.05	-7.2	-7.70	-7.10	-7.46	-7.30	-2 to -4
GI absorption	Low	Low	High	Low	High	Low	Low	High
P-gp substrate	No	No	Yes	No	Yes	No	No	No
P-gp I Inhibitor	No	No	No	No	No	No	No	No
Log Kp (skin permeation) (cm/s)	0.36	-4.15	-4.86	-4.32	-5.04	-2.74	-2.92	< -5.0
$F_{20\%}$	Low	High	Low	Low	Low	Low	Low	High
$F_{30\%}$	High	High	Low	Low	Low	Low	Low	High
Distribution								
PPB (%)	98.510	96.332	97.953	97.236	98.732	98.671	98.963	<90
BBB Permeability	No	No	No	No	No	No	No	No
VD (L/kg)	1.412	0.668	1.577	1.440	1.588	2.408	1.585	0.04-20
Fraction unbound in plasma (%)	0.846	1.343	1.763	1.807	1.149	1.573	1.148	> 5
Metabolism								
CYP1A2 inhibitor	No	No	No	No	No	No	No	No
CYP2C19 inhibitor	No	Yes	No	No	No	No	No	No
CYP2C9 inhibitor	No	No	No	No	No	Yes	No	No
CYP2D6 inhibitor	No	No	No	No	No	No	No	No
CYP3A4 inhibitor	No	No	No	No	No	No	No	No
CYP1A2 substrate	No	No	No	No	No	Yes	Yes	No
CYP2C19 Substrate	No	No	Yes	Yes	Yes	Yes	Yes	No
CYP2C9 Substrate	Yes	No	No	No	No	No	No	No
CYP2D6 Substrate	No	No	No	No	No	Yes	Yes	No
CYP3A4 Substrate	No	No	Yes	No	No	Yes	Yes	No
Excretion								
Total Clearance (mL/min/kg)	4.830	8.294	4.455	5.939	5.095	15.958	16.356	> 5
Half life	0.070	0.725	0.017	0.016	0.016	0.014	0.010	< 0.3
Toxicity								
AMES toxicity	No	No	No	No	No	No	No	No

ADMET Property	Isolated compound							Acceptable values
	1	2	3	4	5	6	7	
hERG blockers	Yes	No	No	No	No	No	No	No
Hepatotoxicity	No	No	No	No	No	No	No	No
Skin sensitization	Yes	Yes	Yes	No	No	No	No	No
Physicochemical properties (Lipinski Rule Violations) Number of hydrogen bond donors (N-H, O-H): 0 to 7, Number of hydrogen bond acceptors (N, O): 0 to 12, Molecular weight (MW): <500 Da, The logarithm of the n-octanol/water distribution coefficient (Log P): 0 to 3	No; 2 violations: MW>500, Log P>3	Yes; 0 violation	Yes; 1 violation: MW>500	Yes; 1 violation: MW>500	Yes; 1 violation: MW>500	Yes; 1 violation: Log P>3	Yes; 1 violation: Log P>3	< 2 violation

VD: Volume of distribution, PPB: Plasma protein binding, CL: Renal Clearance, F20%: Human oral bioavailability 20%, F30%: Human oral bioavailability 30%, Numbers 1-7 correspond to the isolated compounds listed in Table 5. Acceptable values are according to the software https://admetmesh.scbdd.com.

2,3-dihydroxypropyltriacontanoate (1) showed antibacterial activity against *P. aeruginosa* and *E. coli* with MIC of 312.5 and 312.5 µg/mL, respectively, and minimum bactericidal concentration greater than 312.5 µg/mL [18]. Stigmasterol 3-O-β-D-glucopyranoside (3), which was also isolated from *Wissadula periplocifolia* was the compound responsible for the antibacterial activity of this plant extract against *Enterococcus feacalis* [48]. Spinasterol 3-O-β-D-glucopyranoside (5) was reported to exhibit antibacterial activity against *E. coli, P. aeruginosa,* and *Salmonella typhi* with MIC of 128, 64, and 64 µg/mL, respectively [49]. No antimycobacterial activity of these three compounds has been previously reported. Spinasterol or stigmasta-7,22-diene-3β-ol (7) showed good antibacterial activity against *E. coli, Bacillus subtilis, Klebsiella pneuomoniae, Pseudomonas stutzeri*, and *S. aureus* with MIC of 312, 58, 78, 195 and 9.7 µg/mL, respectively [50]. It also showed good activity against antibiotic (clarithromycin, metronidazole, and levofloxacin)-resistant strains of *Helicobacter pylori* with MIC of 20-80 µg mL [51]. α-spinasterol showed antibacterial activity against *S. pneumoniae, E. coli, S. aureus,* and *Salmonella pullorum* with MIC of 246.15, 275.69, 246.15, and 295.38 µg/mL, respectively [52].

4.2. Molecular interactions of the isolated compounds with selected mycobacterial targets.

4.2.1. ATP synthase.

Mycobacterial ATP synthase is a validated drug target, and compounds inhibiting this enzyme are promising drug candidates [53]. ATP synthase consists of a membrane-embedded part (F_0) that transfers protons from the periplasm to the cytoplasm and a hydrophilic part (F1) where ATP synthesis occurs. The passage of H^+ ions causes the electrochemical gradient that results in ATP synthesis. This property makes ATP synthase enzyme an attractive antimycobacterial drug target [54]. A unique feature of mycobacterial ATP synthase is that it suppresses the ATP hydrolase activity and is unable to create a proton gradient. By doing so, ATP synthase prevents the waste of ATP during low oxygen conditions [55]. Bedaquiline is an approved antitubercular drug that inhibits ATP synthase. This prevents the release of energy for the mycobacterial cellular activities resulting in the death of the mycobacterium [56]. The

binding site of ATPase is largely conserved in mycobacteria. The α subunit from M. tuberculosis shows 55% and 52% sequence identity compared with the homolog in humans and E. coli and mitochondria, respectively.

On the other hand, the β subunit has a 61% and 59% sequence identity compared with the homolog in humans and E. coli and mitochondria, respectively. In the F1-ATPases of M. tuberculosis, the P-loop for nucleotide binding (βG171–T178) and the acidic residue acting as a nucleophile for the ATP hydrolysis reaction (βE183) are highly conserved [53]. The native crystallized ligand interacts in the binding site mainly via hydrophobic interactions with amino acids Val 263, Glu255, Leu 260, Val772, Ile267, Phe 776, Val 263, and Phe 256.
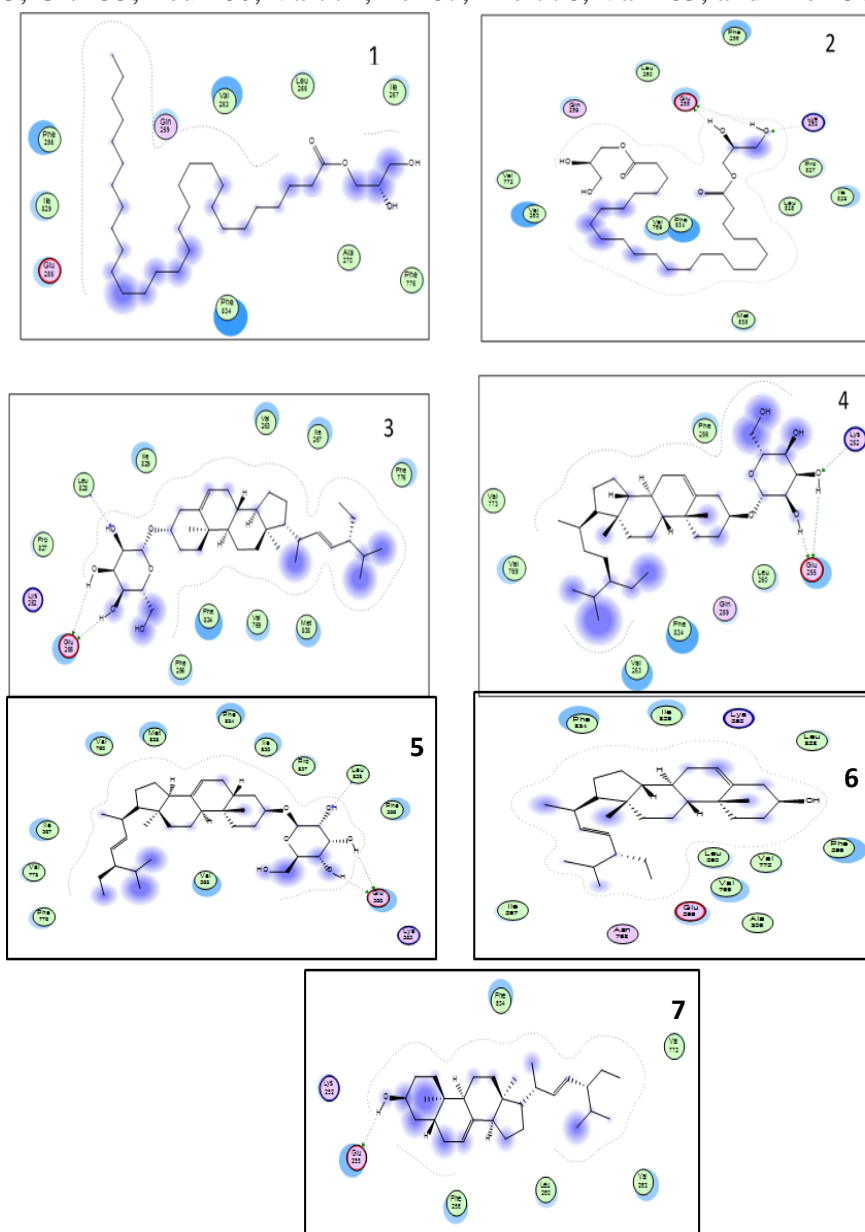
Figure 5. Binding interactions of selected isolated compounds with amino acids in the binding site of ATP synthase. Numbers correspond to compounds isolated.

Two isolated compounds (**1** and **2**) had better binding affinities than the standard drug (bedaquiline) for the ATP synthase enzyme (Table 5). All the isolated compounds had better binding affinities than the two drugs (isoniazid and rifampicin), which form the backbone of any TB regimen (Table 5). Analysis of the binding interactions of the isolated compounds with the amino acids in the binding site of ATP synthase indicated that the ligand formed hydrogen

bonds with amino acid Glu 255 as well as hydrophobic interactions with the close contact amino acid residues (Figure 5). Structurally, compounds **1** and **2** consist of long alkyl chains with a terminal carboxylic acid group. These effectively interact with the amino acids in the catalytic site, dissipating the proton motive force (PMF), which decreases the synthesis of ATP. By doing so, compounds **1** and **2** act as uncouplers of oxidative phosphorylation. SQ109 (Sequella) is a 1,2-ethylenediamine-based compound in phase II clinical trials in South Africa and Russia for a possible antitubercular drug. Structure-activity relationships revealed that the potent antimycobacterial activity of SQI09 and analogs was attributed to its highly α-branched aliphatic moieties, effectively suppressing the PMF and inhibiting ATP synthesis [55]. These compounds also showed moderate activity against two enzymes of the menaquinone biosynthesis pathway, MenA, and MenG, which are critical in synthesizing cofactors for energy production [55]. Hydrolysis of pyrazinamide (a standard drug for TB) to pyrazinoic acid resulted in the dissipation of the PMF and hence inhibition of ATP synthesis in *M. tuberculosis* [55]. Thus, since compounds **1** and **2** contain carboxylic acid moieties on long alkyl groups, it is highly probable that the two compounds interact in synergy with several amino acids in the binding site of ATP synthase and inhibit the PMF, thus reducing the synthesis of ATP.

4.2.2. Polyketide -13 synthase (pks-13).

In mycobacterium, pks-13 enzyme catalyzes the condensation reaction (last step) in the biosynthesis of the mycolic acid required to form the mycobacterial cell wall. Mycolic acids are long α-alkyl, β-hydroxy fatty acids consisting of 60–90 carbon atoms. The mycolic acids covalently interact with the arabinogalactan-peptidoglycan molecules to form the mycolyl-arabinogalactan-peptidoglycan complex. In addition, they also interact with the outer cell envelope lipids, such as trehalose dimycolate (TDM), trehalose monomycolate (TMM), and glucose monomycolate. These interactions make the cell walls of mycobacterium very unique and not easily penetrated by chemotherapeutic agents [57]. Given the critical role of mycolic acids in mycobacterium cell viability and pathogenesis, enzymes involved in mycolic acid biosynthesis, such as PKS13 present novel targets for drug development. The active site of pks-13 is situated at the interface of the core and lid domains, while the substrate-binding pocket is a deep hydrophobic pocket extension from the active site spanning the full length of the lid domain[58]. The co-crystallized ligand in the 5V3Y crystal complex binds in the groove of the fatty acyl chain at the entrance of the active site, thereby inhibiting the substrate from accessing the catalytic binding site. The ligand interacts particularly with the amino acids Phe 1670 (π-π), Glu 1633 (hydrogen bonding), His 1632 (hydrogen bonding), Asn 1640 (hydrogen bonding), Try 1674(π-π), and Asp 1644 (hydrogen bonding) [58].

Five isolated compounds (**1-5**) from *E. abyssinica* had better binding affinities than the standard drugs (isoniazid and rifampicin) on pks-13 target. Compound **1** had the highest binding affinity for the pks-13, while all the sterols had comparable binding affinities to rifampicin (Table 5). With the exception of compound **6,** the other six compounds (**1-5**, **7**) had better binding affinities than isoniazid (a known mycobacterial cell wall synthesis inhibitor). Bedaquiline, however, had a better binding affinity than all the isolated compounds. A visual inspection of the binding interactions suggested that the isolated compounds interacted with amino acid Asn 1640 and other amino acid residues of the binding site of the pks-13 via hydrogen bonding and hydrophobic interactions (Figure 6). In a study to evaluate the antimycobacterial activity of a series of 3,5-disubstituted-1,2,4-oxadiazole derivatives, pks-13

synthase was used as a putative molecular target [58]. Like in this study, the ligands exhibited comparable binding affinities with the standard drugs. Contrary to this study, the major stabilizing interactions between the ligands and the molecular targets were π-π interactions with the amino acids Tyr1637, Tyr1674, Phe1590, Phe1585, Phe1670, and His1699 with some hydrogen bonding with Asn1640 and Ser1636 [58]. Like in this study, five new benzofuran derivatives were reported to have had a sufficient binding affinity for the pks-13 synthase with an alternative binding mode to the active site [15].
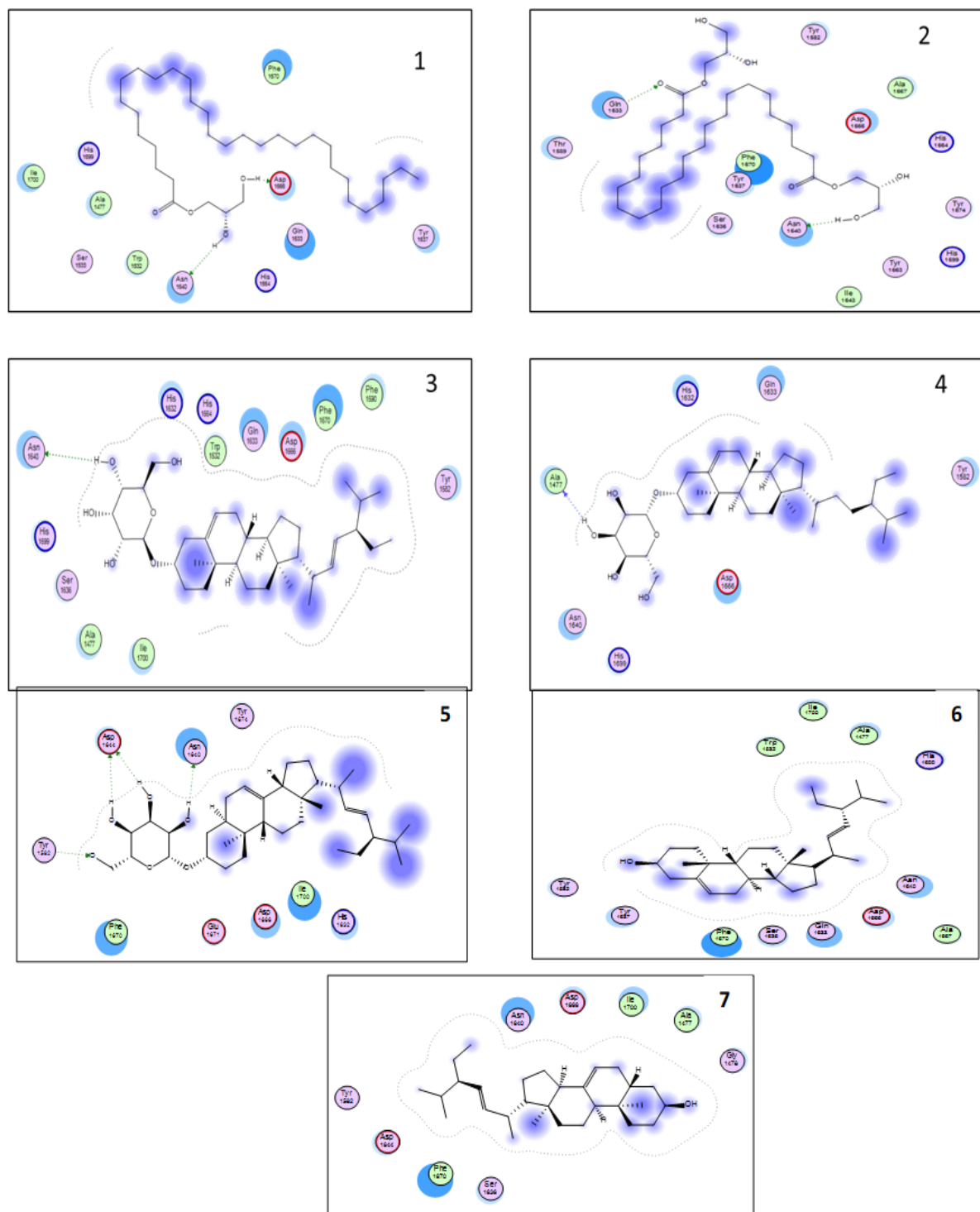
Figure 6. Binding interactions of selected isolated compounds with amino acids in the binding site of Polyketide synthase. Numbers correspond to compounds isolated.

4.3. Pharmacokinetic and toxicity evaluation (ADMET descriptors).

Evaluation of the drug-like properties of promising natural products using *in silico* methods reduces the chances of drug failure during the process of drug development. Only when the ADMET properties of a promising compound are of optimal quality is when the compound could be developed into a new drug [59]. All the compounds had acceptable physicochemical properties with acceptable violations of the Lipinski Rules except compound 1, which had two violations. With the exception of compounds **2, 6,** and **7**, the rest had their molecular weights greater than 500 Da. All the isolated compounds had poor water solubility with their LogS greater than -4.0 (optimum ranges between -2 and -4.0). Therefore, unless optimized to increase their water solubility, this can greatly hinder their absorption as they need to first dissolve in water to be absorbed [60]. This was supported by the calculated parameter of human intestinal absorption, which indicated that most of the compounds had low gastrointestinal absorption. All the compounds were not inhibitors of the P-glycoproteins (P-gp). Except for compounds **3** and **5**, the rest were not substrates of the P- glycoproteins (Table 6). This P-gp is an efflux pump that actively pumps drugs out of the cells, thereby reducing their intracellular concentrations [16]. High expression levels of P-gp are found in normal tissues such as the liver, kidneys, pancreas, adrenal cortex, and colon. In tumor tissues, there is an increase in the expression of P-gp, which results in resistance to multiple drugs due to the increased efflux of the drugs. Physiologically, P-gp has a fundamental role in the secretory processes [16].

All the compounds had high plasma protein binding (greater than 90%) and acceptable volumes of distribution. High protein binding might cause these compounds to have a narrow therapeutic index which is pharmacokinetically undesirable. All the compounds showed low penetration through the blood-brain barrier, suggesting that they could not reach the brain tissues. The blood−brain barrier (BBB) prevents small molecules (98%) and larger molecules (100%) from entering the central nervous system (CNS). However, BBB selectively transports some water-and lipid-soluble molecules and drugs, particularly those that are substrates of P-gp and glucose and transporters [61].

The majority of the compounds were not enzyme inhibitors and thus did not affect the major Cytochrome P450 (CYP450) enzymes. With the exception of compounds **1** and **2**, the rest were substrates for CYP2C19. Compounds **6** and **7** were substrates for all the tested enzymes except CYP2C9. CYP 450 enzymes are a class of mixed functional oxidases primarily located in the liver and intestine that metabolize 60% of xenobiotics. The enzymes mainly catalyze reductions, oxidation, hydrolysis, and epoxidation reactions that transform the parent compound into either less or more active (toxic) metabolites. CYP450 enzymes can either be induced or inhibited by various drugs and substances, resulting in drug-drug interactions that lead to toxicity or decreased therapeutic benefit.

With the exception of compounds **1** and **3**, the rest of the compounds showed acceptable clearance rates from the body Clearance affects both the half-life and bioavailability of drugs, thereby directly influencing the dose and dosing frequency regimen of a drug [16]. The estimation of clearance is important in determining the feasibility of dosing in humans and provides a guide for determining the starting dose in animal and human studies. With the exception of compound **2**, the probability that the rest of the isolated compounds had a half-life of fewer than 3 hours was very low (less than 0.3). This implies that these compounds, if developed into drugs, don't require frequent dosing as the chances of them having longer half-lives were high [62].

Regarding toxicity parameters, most compounds had acceptable toxicity indices with no chances of causing mutagenicity, cardiovascular toxicity, hepatotoxicity, and dermal toxicity. However, compound **1** was more likely to cause cardiovascular and dermal toxicity, while compounds **2** and **3** have high chances of causing dermal toxicity. A close analysis of the ADMET results implies that the isolated compounds possess promising pharmacokinetic properties with minimum toxicity. Hence, the most active compounds could be considered potential drug candidates worthy of undergoing further optimization and validation.

4. Conclusions

E. abyssinica stem bark contains phytochemicals with promising antimycobacterial activity via inhibition of the ATP and polyketide-13 synthase enzymes. *In vitro* and *in vivo* studies are recommended to validate the predicted antimycobacterial activity as well as the pharmacokinetics and toxicity profiles.

Funding

Acknowledgments

Conflicts of Interest

The authors declare no conflict of interest.

References

1. Bostanghadiri, N.; Jazi, F. M.; Razavi, S.; Fattorini, L.; Darban-Sarokhalil, D. Mycobacterium tuberculosis and SARS-CoV-2 Coinfections: A Review. *Front microbiol* **2022,** *12*, 747827, https://doi.org/10.3389/fmicb.2021.747827.
2. World Health Organization. Global Tuberculosis Report **2021**, Geneva, Switzerland.
3. Perveen, S.; Kumari, D.; Singh, K.; Sharma, R. Tuberculosis drug discovery: Progression and future interventions in the wake of emerging resistance. *Eur J Med Chem* **2022**, *229*, 114066, https://doi.org/10.1016/j.ejmech.2021.114066.
4. Gill, C.M.; Dolan, L.; Piggott, L.M.; McLaughlin, A.M. New developments in tuberculosis diagnosis and treatment. *Breathe* **2022**, *18*, 210149, https://doi.org/10.1183/20734735.0149-2021.

5. Omara, T. East African quintessential plants claimed to be used as blood purifiers, cleansers, detoxifiers and tonics: an appraisal of ethnobotanical reports and correlation with reported bioactivities. *Bull Natl Res Cent* **2021**, *45*, 171, https://doi.org/10.1186/s42269-021-00637-4.

6. Obakiro, S.B.; Kiprop, A.; Kigondu, E.; K'Owino, I.; Odero, M.P.; Manyim, S.; Omara, T.; Namukobe, J.; Owor, R.O.; Gavamukulya, Y.; Bunalema, L. Traditional Medicinal Uses, Phytoconstituents, Bioactivities, and Toxicities of *Erythrina abyssinica* Lam. ex DC. (Fabaceae): A Systematic Review. *Evid Based Complement Alternat Med* **2021**, *2021*, 5513484, https://doi.org/10.1155/2021/5513484.

7. Obakiro, S.B.; Kiprop, A.; Kowino, I.; Kigondu, E.; Odero, M.P.; Omara, T.; Bunalema, L. Ethnobotany, ethnopharmacology, and phytochemistry of traditional medicinal plants used in the management of symptoms of tuberculosis in East Africa: a systematic review. *Trop Med Health* **2020**, *48*, 68, https://doi.org/10.1186/s41182-020-00256-1.

8. Tugume, P.; Kakudidi, E.K.; Buyinza, M.; Namaalwa, J.; Kamatenesi, M.; Mucunguzi, P.; Kalema, J. Ethnobotanical survey of medicinal plant species used by communities around Mabira Central Forest Reserve, Uganda. *J ethnobiol ethnomed* **2016**, *12*, 5, https://doi.org/10.1186/s13002-015-0077-4.

9. Melong, R.; Kapche, D.G.; Feussia, M.T.; Laatsch, H. A New Aggreceride analogue and a peltogynoid isolated from the stem bark of *Entada abyssinica* (Fabaceae). *Nat Prod Comm* **2014**, *9*, 1499–1502.

10. Tchinda, A.T.; Fuendjiep, V.; Mekonnen, Y.; Ngo, B.B.; Dagne, E. A Bioactive Diterpene from *Entada abyssinica*. *Nat Prod Comm* **2007**, *2*, 9–12, https://doi.org/10.1177/1934578X0700200103.

11. Dzoyem, J.P.; Melong, R.; Tsamo, A.T.; Tchinda A.T.; Kapche, D.G.W.F.; Ngadjui, B.T.; McGaw, L.J.; Eloff, J.N. Cytotoxicity, antimicrobial and antioxidant activity of eight compounds isolated from *Entada abyssinica* (Fabaceae). *BMC Res Notes* **2017**, *10*, 118, https://doi.org/10.1186/s13104-017-2441-z.

12. Magnibou, L.M.; Leutcha, P.B.; Tchegnitegni, B.T.; Wouamba, S.C.N.; Magne, C.Y.F.F.; Yaya, A.J.G.; Kopa, T.; Tagatsing, M.F.; Tombozara, N.; Meli, A.L.; Henoumont, C.; Laurent, S.; Talla, E. A new phenanthrene derivative from *Entada abyssinica* with antimicrobial and antioxidant properties. *Zeitschrift für Naturforschung B* **2022,** *77*, 1-7, https://doi.org/10.1515/znb-2021-0076.

13. Mariita, R.M.; Orodho, J.A.; Okemo, P.O.; Mbugua, P.K. Antifungal, antibacterial and antimycobacterial activity of Entada abysinnica Steudel ex A . Rich (Fabaceae) methanol extract. *Pharmacog Res* **2010**, *2*, 163–168, https://doi.org/10.4103/0974-8490.655111.

14. Omara, T.; Kiprop, A.K.; Kosgei, V.J. *Albizia coriaria* Welw ex Oliver: a review of its ethnobotany, phytochemistry and ethnopharmacology. *Adv Tradit Med* **2021**, https://doi.org/10.1007/s13596-021-00600-8.

15. Obakiro, S.B.; Kiprop, A.; K'owino, I.; Andima, M.; Owor, R.O.; Chacha, R.; Kigondu, E. Phytochemical, Cytotoxicity, and Antimycobacterial Activity Evaluation of Extracts and Compounds from the Stem Bark of *Albizia coriaria* Welw ex. Oliver. *Evid Based Complement Alternat Med* **2022**, *2022*, 7148511, https://doi.org/10.1155/2022/7148511.

16. Durán-Iturbide, N.A.; Díaz-Eufracio, B.I.; Medina-Franco, J.L. *In Silico* ADME/Tox Profiling of Natural Products: A Focus on BIOFACQUIM. *ACS Omega* **2020**, *5*, 16076–16084, https://doi.org/10.1021/acsomega.0c01581.

17. Konappa, N.; Udayashankar, A.C.; Krishnamurthy, S.; Pradeep, C.K.; Chowdappa, S.; Jogaiah, S. GC-MS analysis of phytoconstituents from Amomum nilgiricum and molecular docking interactions of bioactive serverogenin acetate with target proteins. *Sci Rep* **2020**, *10*, 16438, https://doi.org/10.1038/s41598-020-73442-0.

18. Teke, G.N.; Lunga, P.K.; Wabo, H.K.; Kuiate, J.; Vilarem, G.; Giacinti, G.; Kikuchi, H.; Oshima, Y. Antimicrobial and antioxidant properties of methanol extract, fractions and compounds from the stem bark of Entada abyssinica Stend ex A. Satabie. *BMC Complement Altern Med* **2011** *11*, 57, https://doi.org/10.1186/1472-6882-11-57.

19. Yang, N.-Y.; Tao, W.-W.; Duan, J.-A. Three new lipids from the seeds of Trogopterus xanthipes. *J Chem Res* **2009**, *7,* 423–426, https://doi.org/10.3184/030823409X465330.

20. Kojima, H.; Sato, N.; Hatano, A.; Ogura, H. Sterol glucosides from *Prunella vulgaris*. *Phytochem* **1990**, *29*, 2351–2355, https://doi.org/10.1016/0031-9422(90)83073-A.

21. Sandjo, L.P., Kuete, V. Triterpenes and Steroids from the Medicinal Plants of Africa. *In; Medicinal Plant Research in Africa: Pharmacology and Chemistry* **2013**, Elsevier, 135–202, https://doi.org/10.1016/B978-0-12-405927-6.00004-7.

22. Hernández-García, E.; García, A.; Avalos-Alanís, F.G.; Rivas-Galindo, V.M.; Delgadillo-Puga, C.; Camacho-Corona, M. Nuclear magnetic resonance spectroscopy data of isolated compounds from Acacia

farnesiana (L) Willd fruits and two esterified derivatives. *Data Brief* **2018**, *22*, 255–268, https://doi.org/10.1016/j.dib.2018.12.008.

23. Agrawal, P.K.; Jain, D.C. 13C NMR spectroscopy of oleanane triterpenoids. *Prog Nucl Magn Res Spect* **1992**, *24*, 1–90, https://doi.org/10.1016/0079-6565(92)80011-4.

24. Hernández-García, E.; García, A.; Garza-González, E.; Avalos-Alanís, F.G.; Rivas-Galindo, V.M.; Rodríguez-Rodríguez, J.; Alcantar-Rosales, V.M.; Delgadillo-Puga, C.; del Rayo Camacho-Corona, M. Chemical composition of Acacia farnesiana (L) wild fruits and its activity against Mycobacterium tuberculosis and dysentery bacteria. *J Ethnopharmacol* **2019**, *230*, 74–80, https://doi.org/10.1016/j.jep.2018.10.031.

25. Gu, X.; Li, Y.; Mu, J.; Zhang, Y. Chemical constituents of *Prunella vulgaris*. *J Environ Sci* **2013**, *25*, S161–S163, https://doi.org/10.1016/S1001-0742(14)60648-3.

26. Dinda, B.; Ghosh, B.; Achari, B.; Arima, S.; Sato, N.; Harigaya, Y. Chemical constituents of Gomphrena globosa II. *Nat Prod Sci* **2006**, *12*, 89–93.

27. Afrizal, S.; Efdi, M. Isolation and elucidation structure of stigmasterol glycoside from Nothopanax scutellarium Merr leaves. *J Chem Pharm Res* **2015**, *7,* 763–765.

28. Peshin, T.; Kar, H. Isolation and characterization of β-sitosterol-3-O-β-D-glucoside from the extract of the flowers of Viola odorata Br. *J Pharm Res Intern* **2017**, *16*, 1–8, https://doi.org/10.9734/bjpr/2017/33160.

29. Rashed, K.; Ćirić, A.; Glamočlija, J.; Calhelha, R.C.; Ferreira, I.C.F.R.; Soković, M. Antimicrobial and cytotoxic activities of Alnus rugosa L. aerial parts and identification of the bioactive components. *Ind Crops Prod* **2014**, *59*, 189-196, https://doi.org/10.1016/j.indcrop.2014.05.017.

30. Ono, M.; Oishi, K.; Abe, H.; Masuoka, C.; Okawa, M.; Ikeda, T.; Nohara, T. New iridoid glucosides from the aerial parts of Verbena brasiliensis. *Chem Pharm Bull* **2006**, *54*, 1421–1424, https://doi.org/10.1248/cpb.54.1421.

31. Henry, M.; Chantalat-Dublanche, I. Isolation of spinasterol and its glucoside from cell suspension cultures of *Saponaria officinalis*: 13C-NMR Spectral Data and Batch Culture Production. *Planta Medica* **1985**, *51*, 322–325, https://doi.org/10.1055/s-2007-969502.

32. Kiuchi, F.; Gafur, A.; Obata, T.; Tachibana, A.; Tsuda, Y. Acacia concinna Saponins. II. Structures of monoterpenoid glycosides in the alkaline hydrolysate of the saponin fraction. *Chem Pharm Bull* **1997**, *45*, 807–812, https://doi.org/10.1248/cpb.45.807.

33. Gade, I.; Chadeneau, C.; Simo, R.; Talla, E.; Atchade, A.; Seité, P.; Vannier, B.; Laurent, S.; Henoumont, C.; Nwabo Kamdje, A; Muller, J. A new phenyl alkyl ester and a new combretin triterpene derivative from Combretum fragrans F. Hoffm (Combretaceae) and antiproliferative activity. *Open Chem* **2020,** *18*, 1523-1531, https://doi.org/10.1515/chem-2020-0167.

34. Meneses-Sagrero, S.E.; Navarro-Navarro, M.; Ruiz-Bustos, E.; Del-Toro-Sánchez, C.L.; Jiménez-Estrada, M.; Robles-Zepeda, R.E. Antiproliferative activity of spinasterol isolated of *Stegnosperma halimifolium* (Benth, 1844). *Saudi Pharm J* **2017**, *25*, 1137–1143, https://doi.org/10.1016/j.jsps.2017.07.001.

35. Ahmed, M.; Qin, P.; Ji, M.; An, R.; Guo, H.; Shafi, J. Spinasterol, 22,23-Dihydrospinasterol and Fernenol from *Citrullus Colocynthis* L. with Aphicidal Activity against Cabbage Aphid *Brevicoryne Brassicae* L. *Molecules* **2020**, *25*, 2184, https://doi.org/10.3390/molecules25092184.

36. Billah, A.H.M.M.; Hussain, M.M.; Dastagir, M.G.; Ismail, M.; Quader, A. Isolation of α-spinasterol from Amaranthus spinosus stems. *Boletín Latinoam. y del Caribe Plantas Med. y Aromáticas* **2013**, *12*, 15–17.

37. Jeong, S.I.; Kim, K.J.; Choi, M.K.; Keum, K.S.; Lee, S.; Ahn, S.H.; Back, S.H.; Song, J.H.; Ju, Y.S.; Choi, B.K.; Jung, K.Y. alpha-Spinasterol isolated from the root of Phytolacca americana and its pharmacological property on diabetic nephropathy. *Planta medica* **2004**, *70*, 736–739, https://doi.org/10.1055/s-2004-827204.

38. Alderwick, L.J.; Harrison, J.; Lloyd, G.S.; Birch, H.L. The Mycobacterial Cell Wall--Peptidoglycan and Arabinogalactan. *Cold Spring Harb Perspect Med* **2015**, *5*, a021113. https://doi.org/10.1101/cshperspect.a021113

39. Deb, P.K.; Al-Shar'i, N.A.; Venugopala, K.N.; Pillay, M.; Borah, P. *In vitro* anti-TB properties, *in silico* target validation, molecular docking and dynamics studies of substituted 1,2,4-oxadiazole analogues against *Mycobacterium tuberculosis*. *J Enzyme Inhib Med Chem* **2021**, *36*, 869–884, https://doi.org/10.1080/14756366.2021.1900162.

40. Montgomery, M.G.; Petri, J.; Spikes, T.E.; Walker, J.E. Structure of the ATP synthase from *Mycobacterium smegmatis* provides targets for treating tuberculosis. *PNAS* **2021,** *118*, e2111899118, https://doi.org/10.1073/pnas.2111899118.

41. Hasenoehrl, E.J.; Wiggins, T.J.; Berney, M. Bioenergetic Inhibitors: Antibiotic Efficacy and Mechanisms of Action in *Mycobacterium tuberculosis*. *Front Cell Infect Microbiol* **2021**, *10*, 611683, https://doi.org/10.3389/fcimb.2020.611683.

42. Appetecchia, F.; Consalvi, S.; Scarpecci, C.; Biava, M.; Poce, G. SAR Analysis of Small Molecules Interfering with Energy-Metabolism in *Mycobacterium tuberculosis*. *Pharmaceuticals* **2020**, *13*, 227, https://doi.org/10.3390/ph13090227.

43. Novoa-Aponte, L.; Soto Ospina, C.Y. *Mycobacterium tuberculosis* P-type ATPases: possible targets for drug or vaccine development. *BioMed Res Int* **2014**, *2014*, 296986, https://doi.org/10.1155/2014/296986.

44. Messanga, R.E.; Ngono, B.D.E.; Zintchem, A.A.A.; Mbabi, N.N.; Del Florence, M.N.E.; Betote, D.P.H.; Nyegue, M.A.; De Théodore, A.A.; Pegnyemb, D.E.; Bochet, C.G.; Koert, U. Rauvolfianine, a new antimycobacterial glyceroglycolipid and other constituents from *Rauvolfia caffra*. Sond (Apocynaceae). *Nat Prod Res* **2018**, *32*, 1971–1976, https://doi.org/10.1080/14786419.2017.1356832.

45. Wong, K.C.; Hag Ali, D.M.; Boey, P.L. Chemical constituents and antibacterial activity of *Melastoma malabathricum* L. *Nat Prod Res* **2012**, *26*, 609–618, https://doi.org/10.1080/14786419.2010.538395.

46. Mbosso, T.J.E.; Ngouela, S.; Nguedia, J.C.A.; Beng, V.P.; Rohmer, M.; Tsamo, E. Spathoside, a cerebroside and other antibacterial constituents of the stem bark of Spathodea campanulata. *Nat Prod Res* **2008**, *22*, 296–304, https://doi.org/10.1080/14786410701766281.

47. Subramaniam, S.; Keerthiraja, M.; Sivasubramanian, A. Synergistic antibacterial action of β -sitosterol- D -glucopyranoside isolated from Desmostachya bipinnata leaves with antibiotics against common human pathogens. *Rev Bras Farmacogn* **2014**, *24*, 44-50, https://doi.org/10.1590/0102-695X20142413348.

48. Kazakova, O.; Racoviceanu, R.; Petrova, A.; Mioc, M.; Militaru, A.; Udrescu, L.; Udrescu, M.; Voicu, A.; Cummings, J.; Robertson, G.; Ordway, D.J.; Slayden, R.A.; Șoica, C. New Investigations with Lupane Type A-Ring Azepane Triterpenoids for Antimycobacterial Drug Candidate Design. *Int J Mol Sci* **2021**, *22*, 12542, https://doi.org/10.3390/ijms222212542.

49. Suja, K.; Leny, J.; Divya, L.; Anu, V.G.; Reshmi, R.N.; Kumar, R.A. Isolation and Characterization of Antimycobacterial Compounds from Fruits of Aegle marmelos (L.) Correa. *J Comm Dis* **2017**, *49*, 32-38.

50. Salih, E.; Julkunen-Tiitto, R.; Lampi, A.M.; Kanninen, M.; Luukkanen, O.; Sipi, M.; Lehtonen, M.; Vuorela, H.; Fyhrquist, P. *Terminalia laxiflora* and *Terminalia brownii* contain a broad spectrum of antimycobacterial compounds including ellagitannins, ellagic acid derivatives, triterpenes, fatty acids and fatty alcohols. *J Ethnopharmacol* **2018**, *227*, 82–96, https://doi.org/10.1016/j.jep.2018.04.030.

51. Salih, E.; Julkunen-Tiitto, R.; Luukkanen, O.; Sipi, M.; Fahmi, M.; Fyhrquist, P.J. Potential Anti-Tuberculosis Activity of the Extracts and Their Active Components of *Anogeissus Leiocarpa* (DC.) Guill. and Perr. with Special Emphasis on Polyphenols. *Antibiotics* **2020**, *9*, 364, https://doi.org/10.3390/antibiotics9070364.

52. Alawode, T.T.; Lajide, L.; Olaleye, M.; Owolabi, B. Stigmasterol and β-Sitosterol: Antimicrobial Compounds in the Leaves of *Icacina trichantha* identified by GC–MS. *Beni-Suef Univ J Basic Appl Sci* **2021**, *10*, 80, https://doi.org/10.1186/s43088-021-00170-3.

53. Edilu, A.; Adane, L.; Woyessa, D. In vitro antibacterial activities of compounds isolated from roots of Caylusea abyssinica. *Ann Clin Microbiol Antimicrob* **2015**, *14*, 15, https://doi.org/10.1186/s12941-015-0072-6.

54. Teles, Y.C.F.; Chaves, O.S.; Agra, M. et al. Chemical constituents from *Sidastrum paniculatum* and evaluation of their leishmanicidal activity. *Rev Bras Farmacogn* **2015**, *25*, 363-368, https://doi.org/10.1016/j.bjp.2015.02.002.

55. Nyem, J.N.; Tchinda, A.T.; Talla, E. et al. Vitellaroside, A New Cerebroside from Vitellaria paradoxa (Sapotaceae) and its Bioactivities. *Nat Prod Chem Res* **2018**, *6*, 306, http://dx.doi.org/10.4172/2475-7675.1000306.

56. Amir, F.; Wong, K.C.; Eldeen, I.; Asmawi, M.Z.; Osman, H. Evaluation of Biological Activities of Extracts and Chemical Constituents of *Mimusops elengi*. *Trop J Pharm Res* **2013**, *12*, 591-596, https://doi.org/10.4314/tjpr.v12i4.22.

57. Wang, Y. C.; Li, W.Y.; Wu, D.C.; Wang, J.J.; Wu, C.H.; Liao, J.J.; Lin, C.K. *In Vitro* Activity of 2-methoxy-1,4-naphthoquinone and Stigmasta-7,22-diene-3β-ol from Impatiens balsamina L. against Multiple Antibiotic-Resistant *Helicobacter pylori*. *Evid Based Complement Alternat Med* **2011**, *2011*, 704721, https://doi.org/10.1093/ecam/nep147.

58. Yang, X.; Zhou, J.; Wang, T.; Zhao, L.; Ye, G.; Shi, F.; Li, Y.; Tang, H.; Dong, Q.; Zhou, X.; Xu, M.; Rong, Q.; Chen, H.; Yang, X.; Cai, Y. A novel method for synthesis of α-spinasterol and its antibacterial activities in combination with ceftiofur. *Fitoterapia* **2017**, *119*, 12–19, https://doi.org/10.1016/j.fitote.2017.03.011.

59. Wu, F.; Zhou, Y.; Li, L.; Shen, X.; Chen, G.; Wang, X.; Liang, X.; Tan, M.; Huang, Z. Computational Approaches in Preclinical Studies on Drug Discovery and Development. *Front Chem* **2020**, *8*, 726, https://doi.org/10.3389/fchem.2020.00726.

60. Hoti, G.; Matencio, A.; Rubin Pedrazzo, A.; Cecone, C.; Appleton, S. L.; Khazaei Monfared, Y.; Caldera, F.; Trotta, F. Nutraceutical Concepts and Dextrin-Based Delivery Systems. *Int J Mol Sci* **2022**, *23*, 4102, https://doi.org/10.3390/ijms23084102.

61. Lagorce, D.; Douguet, D.; Miteva, M.A.; Villoutreix, B.O. Computational analysis of calculated physicochemical and ADMET properties of protein-protein interaction inhibitors. *Sci Rep* **2017**, *7*, 46277, https://doi.org/10.1038/srep46277.

62. Chai, T.T.; Koh, J.A.; Wong, C.C.; Sabri, M.Z.; Wong, F.C. Computational Screening for the Anticancer Potential of Seed-Derived Antioxidant Peptides: A Cheminformatic Approach. *Molecules* **2021**, *26*, 7396, https://doi.org/10.3390/molecules26237396.